Cell. Mol. Life Sci. 65 (2008) 2594 – 2612
1420-682X/08/162594-19
DOI 10.1007/s00018-008-8249-1

Cellular and Molecular Life Sciences

Research Article

Atomic model of human cystic fibrosis transmembrane conductance regulator: Membrane-spanning domains and coupling interfaces

J.-P. Mornon[a, b, c, d], P. Lehn[e, f] and I. Callebaut[a, b, c, d, *]

[a] Université Pierre et Marie Curie-Paris 6, IMPMC-UMR7590, Campus Boucicaut, 140 rue de Lourmel, Paris 75015 (France), Fax: +33-1-4427-3785, e-mail: Isabelle.Callebaut@impmc.jussieu.fr
[b] CNRS, Paris 75016 (France)
[c] Université Paris Diderot-Paris 7, Paris 75013 (France)
[d] Institut de Physique Globe de Paris-IPGP, Paris 75005 (France)
[e] INSERM, U613, Brest 29200 (France)
[f] Université de Bretagne Occidentale, Brest 29200 (France)

Received 6 May 2008; received after revision 10 June 2008; accepted 11 June 2008
Online First 4 July 2008

Abstract. We describe herein an atomic model of the outward-facing three-dimensional structure of the membrane-spanning domains (MSDs) and nucleotide-binding domains (NBDs) of human cystic fibrosis transmembrane conductance regulator (CFTR), based on the experimental structure of the bacterial transporter Sav1866. This model, which is in agreement with previous experimental data, highlights the role of some residues located in the transmembrane passages and directly involved in substrate translocation and of some residues within the intracellular loops (ICL1–ICL4) making MSD/NBD contacts. In particular, our model reveals that D173 ICL1 and N965 ICL3 likely interact with the bound nucleotide and that an intricate H-bond network (involving especially the ICL4 R1070 and the main chain of NBD1 F508) may stabilize the interface between MSD2 and the NBD1 F508 region. These observations allow new insights into the ATP-binding sites asymmetry and into the molecular consequences of the F508 deletion, which is the most common cystic fibrosis mutation.

Keywords. CFTR, Sav1866, ABC transporters, hydrophobic cluster analysis, cystic fibrosis.

Introduction

The cystic fibrosis transmembrane conductance regulator (CFTR/ABCC7) protein is a phosphorylation-dependent chloride channel [1], which is present at the apical membrane of epithelial cells and belongs to the ATP-binding cassette (ABC) superfamily. More than a thousand naturally occurring CFTR mutations have been reported that lead to cystic fibrosis (CF), the most common fatal recessive genetic disease affecting Caucasian populations [2]. Most of them induce alterations in protein biosynthesis or lead to defective channel function [3]. The most common CF-causing mutation, a deletion of the phenylalanine residue 508 (ΔF508), is responsible for a majority (~70 %) of the CF cases and affects the folding and trafficking of the protein, resulting in its premature degradation.

* Corresponding author.

Full-size ABC transporters have two membrane-spanning domains (MSDs) that allow the transport of compounds across the membrane and two cytoplasmic nucleotide-binding domains (NBDs), which bind and hydrolyze ATP, the energy of which is required for substrate transport. Many eukaryotic ABC exporters like CFTR have all four domains expressed as a single polypeptide chain, whereas bacterial exporters form homo- or heterodimers of "half-transporters", each consisting of an MSD fused to an NBD. A specific feature of CFTR is the presence of a large regulatory (R) domain, which lies between the first NBD (NBD1) and the second MSD (MSD2) and stimulates the ATPase activity and channel gating when phosphorylated by protein kinase A (PKA) [4]. In our previous modeling work, based on the experimental data of well-characterized NBDs from ABC transporters, we described the "head-to-tail" 3-D arrangement of the CFTR NBD1/NBD2 heterodimer, with the two ATP-binding sites located at the interface between the two subunits [5, 6]. Figure 1A shows the principal features of this NBD1/NBD2 heterodimer, within the model of the MSDs:NBDs presented here. Only one ATP-binding site (the NBD2 ATP-binding site, also termed the "canonical" ATP-binding site), which includes the Walker A (P-loop) and Walker B motifs of the second NBD (NBD2) and the signature motif (C-loop) of NBD1, was predicted to be enzymatically active. The non-canonical ATP-binding site (or NBD1 ATP-binding site) lacks the catalytic glutamate in the NBD1 Walker B motif and contains highly modified motifs. Of note, a large loop containing helical extensions (called the β1−β2 loop or the A loop [7], and, in the case of CFTR, also termed the "regulatory insertion" [8]) was found to be located between the two first β-strands of the NBD1 ABC-specific β sub-domain, and it was suggested that it might cover the non-canonical NBD1 ATP-binding site. Our NBD1/NBD2 heterodimer model and the concomitant resolution of NBD1 3-D structures [8, 9] have also revealed that the F508 side chain was exposed at the NBD1 surface, in a position allowing interactions with the MSDs (Fig. 1A). Such a role is in agreement with experimental studies, which have shown that ΔF508 disrupts the packing of the CFTR TM segments [10]. This likely reflects a direct interaction between NBD1 and an MSD, rather than an indirect effect on NBD1/NBD2 association [11], although F508 has been shown to be required for the correct folding of NBD2 [12].

Until recently, modeling of full-length structures of CFTR and other eukaryotic ABC transporters has been slowed down for several reasons. First, in contrast to NBDs for which several high-resolution structures have been published, structural information for MSDs is scarce. Moreover, the sequence, topology and number of transmembrane (TM) helices vary considerably from one transporter to another [13]. The only two structures available until recently were: (i) that of the outward-facing conformation (where the TM pore is accessible from the extracellular side) of the *E. coli* vitamin B12 importer BtuCD, which has ten TM spans per MSD [14], and (ii) those of the MsbA exporters from *E. coli, V. cholerae* and *S. typhimurium*, which, like CFTR, have six TM spans per MSD [15–18]. These latter structures were, however, proven incorrect and consequently withdrawn [19, 20]. It was thus only in 2006 that a correct crystal structure of a full ABC exporter was published. It was that of the multi-drug transporter Sav1866 from *S. aureus* [21] in its outward-facing conformation, and it was quickly recognized that it may serve as a template for modeling the outward configuration of other ABC exporters, including CFTR. Indeed, similarly to Sav1866, these exporters have six long TM helices (per MSD). These largely protrude into the cytoplasm. The resulting intracellular loops (ICLs) contain short 'coupling helices" which run parallel to the plane of the membrane and provide the bulk of the contacts with the NBDs. In particular, a Sav1866-like architecture has been proved, by cysteine mutagenesis and chemical cross-linking experiments, to be maintained in the CFTR-related P-glycoprotein (ABCB1) [22]. Two other structures of full bacterial ABC transporters have also recently been published, but they correspond to inward-facing configurations of importers. The first (*H. influenzae* HI1470/1 [23]) has, like BtuCD, ten TM spans per MSD, whereas the second (*A. fulgidus* ModBC-A [24]) has six TM spans per MSD, but with a topological arrangement distinct from that of Sav1866 (for a review see [13]). Finally, corrected structures of *E. coli*/*V. cholerae* MsbA, trapped in different conformations, were recently republished [25]. Interestingly, while the outward-facing conformation of nucleotide-bound MsbA was found to be quite similar to that of Sav1866, the observed inward-facing conformations were significantly different, a fact allowing new insights into the putative conformational changes occurring upon nucleotide hydrolysis.

The second fact hindering homology modeling is that it is difficult to align the ABC transporter TM regions with great accuracy, due to the low levels of conservation between prokaryotic and eukaryotic sequences. It should be stressed here that, in the recent modeling studies of various ABC transporters (including very recently CFTR) performed using Sav1866 as template [26–30], the sequence alignments were generally performed solely using automatic tools

and were adapted, for consistency purposes, by comparing the observed and predicted secondary structures and/or TM segments. Although such strategies can lead to accurate alignments within the most conserved regions (*e.g.*, in the NBDs or in the ICLs, which are better conserved than the TM segments of MSDs), they are prone to misalignments in the TM segments, where the very low sequence identities do not provide valuable anchors.

Thus, to perform a refined (as far as possible) alignment of the CFTR MSDs with the Sav1866 sequence, we used here the hydrophobic cluster analysis (HCA) method, which has already allowed us in the past to refine the alignment of the CFTR NBD1 N-terminal region, in particular to correctly align the aromatic residue (CFTR W401) involved in $\pi-\pi$ stacking interactions with the adenine ring of the bound nucleotide [5, 6] (Fig. 1A). Our prediction, which was validated by the resolution of the experimental structure of CFTR NBD1 [8, 9], implied that a large insertion (which was termed the "regulatory insertion" [8]) has to be made between the two first β-strands of the NBD1 ABC-specific β sub-domain. Such a level of refinement is generally not attainable by automatic alignment procedures, which indeed led to mispredictions of this essential residue of the so-called A-loop (see for example the prediction made in [7]). The greater sensitivity of HCA, relatively to other methods, results from the fact that it takes into account the conserved topological features of secondary structures in globular domains, but also within TM segments [31–33]. HCA is widely used to analyze and compare sequences of soluble proteins, by exploiting the fundamental dichotomy between hydrophobic and non-hydrophobic residues, which governs their folds. In polytopic membrane proteins, HCA can reveal another essential dichotomy (and associated features at the 2-D level), between hydrophobic and small residues. The latter appear to play a key role in the packing of TM segments [34]. The HCA potential for accurate alignment of highly divergent TM segments has recently clearly been demonstrated by the modeling of the Rh proteins on the basis of the experimental structures of bacterial ammonium transporters [35, 36].

In the present work, we have used (i) the outward-facing configuration of the Sav1866 experimental structure as template and (ii) an HCA-based refined alignment of the MSDs and NBDs, to construct a homology model of the human CFTR MSD1:NBD1:MSD2:NBD2 assembly, its accuracy being evaluated by comparing its features with available physiological and mutagenesis data. Moreover, the contact regions between the MSDs and NBDs were carefully compared with those of the CFTR model recently proposed by Serohijos et al. [31], to highlight important features of these interfaces that have not yet been reported, especially in the vicinity of the F508 residue. In addition, our model also reveals original features of the channel pore formed by the CFTR MSDs. Our Sav1866-based CFTR model allows novel insights into the molecular mechanisms underlying CFTR functioning and it may also help to design future work aiming at a better experimental characterization of this ABC transporter.

Methods

Global strategy

The underlying rationale was to construct our model on the basis of the alignment of the human CFTR sequence (MSDs and NBDs) with the *S. aureus* Sav1866 sequence, to preserve the main interface features between the different domains. Indeed, although the overall features of the crystal structure of the isolated human CFTR NBD1 [8] are highly similar to our Sav1866-based NBD1 model, constructed within the context of the whole MSD:NBD assembly, we have deliberately chosen not to use the crystal structure data, as they may not account for the structural plasticity locally observed at domain interfaces (see Supplementary data 1 for a comparison of both structures; the supplementary data can be downloaded from http://www.impmc.jussieu.fr/~callebau/CFTR.html). Moreover, the orientation of the ABC-specific α subdomain relative to the α/β core in the crystal structure of the isolated human CFTR NBD1 is slightly different from that observed in the Sav1866-based model, which allows an optimal interaction with the MSDs. Finally, artificial contacts between side chains of NBD1 surface residues may exist in the crystal structure of the isolated human CFTR NBD1, which are no longer allowed in the whole assembly (see Discussion).

The model was constructed as a whole using Modeller (release 9v2; [37]) and was further refined on the energetic level using the SwissPDBViewer tools [38]. For comparative purposes, it should be noted here that the recent model proposed by Serohijos et al. [39] (called herein the "hybrid" model) was built by superimposing a NBD1-NBD2 dimer {consisting of the CFTR NBD1 crystal structure (pdb 2bbo) [8] and our previous homology model of human CFTR NBD2 [5, 6]} on the Sav1866 structure [21], which was considered as a template only for modeling of the MSDs. Thus, it is not surprising that such different approaches lead to significant differences in the models proposed, especially as regards the

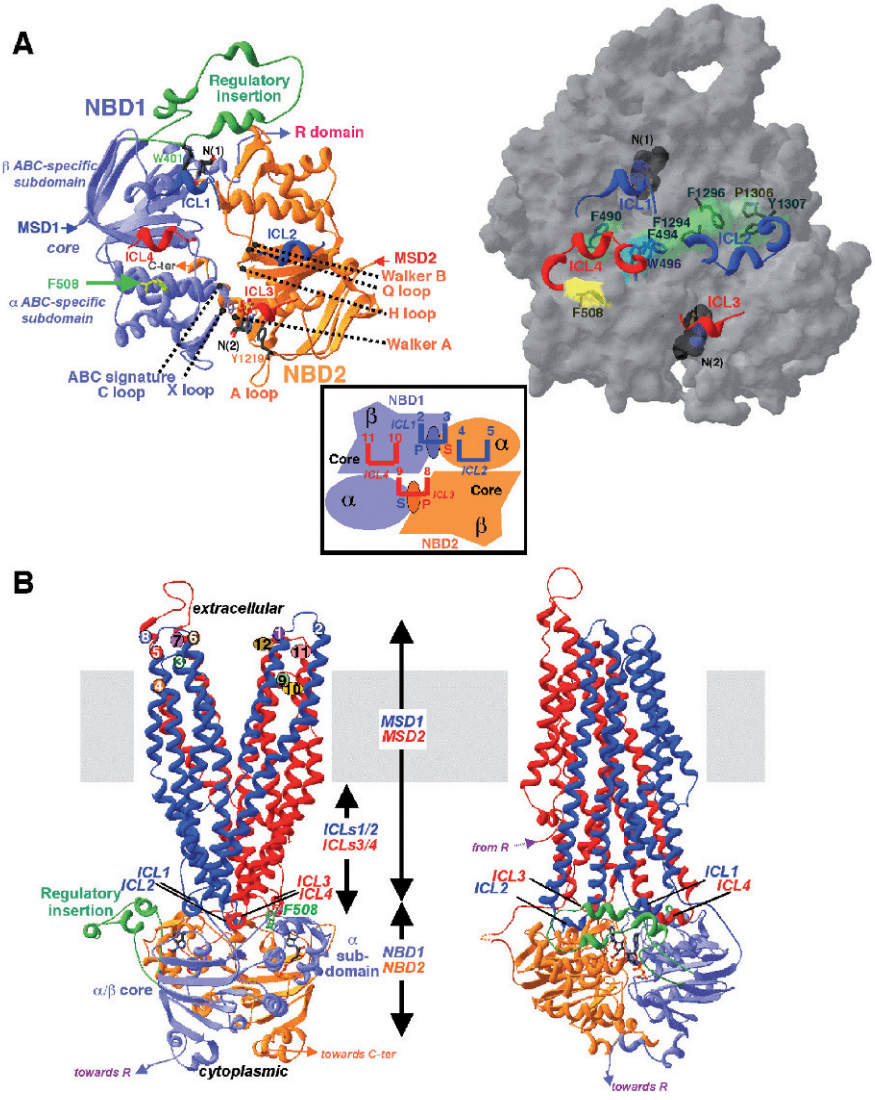

Figure 1. Sav1866-based model of the MSD1:NBD1:MSD2:NBD2 assembly of human CFTR. (A) NBD1:NDB2 heterodimer viewed from the membrane. Left: Ribbon representation. The figure shows the two NBDs (NBD1 in light blue and NBD2 in orange), as well as the coupling helices of the MSD intracellular loops (MSD1 in dark blue and MSD2 in red). Bound ADP molecules [as modeled from the Sav1866 structure and designated N(1) and N(2)] are also shown, the two aromatic residues located at the beginning of the A loops and interacting with the nucleotide adenine rings being indicated. The conserved ABC motifs are depicted for the NBD2 conventional ATP-binding site. The large insertion (termed regulatory insertion) in the β1–β2 loop of the NBD1 ABC-specific β sub-domain, taken from the murine NBD1 experimental structure (pdb 1r0w; [9]), is shown in green (see also Supplementary data 2; http://www.impmc.jussieu.fr/~callebau/CFTR.html). Right: Solvent-exposed surface, highlighting the MSD/NBD interfaces. The ribbon representations of MSD1 ICLs are shown in blue, those of the MSD2 ICLs in red, whereas the solvent exposed surfaces of aromatic residues forming a groove between the core and the ABC-specific α subdomain are shaded green (with F508 in yellow). Inset: Cartoon depicting the positions of the MSD/NBD interfaces. NBD1 and MSD1 ICLs are shown in light and dark blue, respectively, while NBD2 and MSD2 ICLs are shown in orange and red, respectively. Relevant NBD structures are also indicated. (B) Two orthogonal views of the MSD1:NBD1:MSD2:NBD2 assembly (ribbon representation). MSD1 and NBD1 are shown in blue, MSD2 and NBD2 in red/orange. The regulatory insertion is shown in green. MSD: membrane-spanning domain; NBD: nucleotide-binding domain; CFTR: human cystic fibrosis transmembrane conductance regulator; ABC: ATP-binding cassette; core, α and β: core, ABC-specific α and β subdomains; P: P-loop; S: signature motif.

MSDs:NBDs interfaces (see the Results and Discussion section below).

Nucleotide-binding domains

The alignment of the two CFTR NBDs sequences with the Sav1866 NBD sequence is shown in Supplementary data 2 (http://www.impmc.jussieu.fr/~callebau/CFTR.html). This alignment was performed according to our previously reported alignments of the two NBD sequences of human CFTR with those of several ABC transporters of known 3-D structures [5, 6]. In that previous work, a first alignment had permitted an accurate alignment of the aromatic residue (W401) located at the end of NBD1 strand β1, provided that a

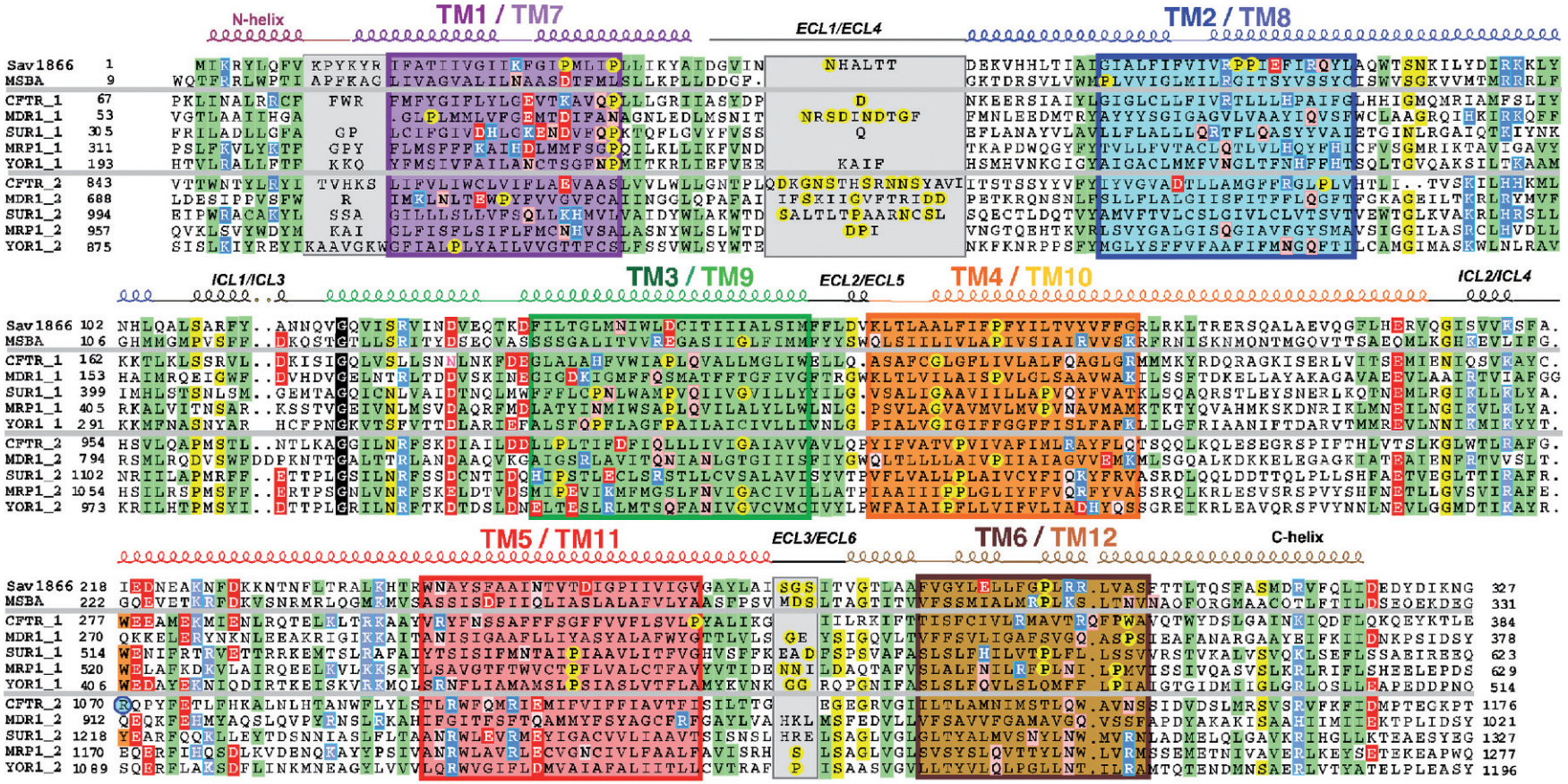

Figure 2. Hydrophobic cluster analysis (HCA)-based sequence alignment of the MSDs of different ABC transporters. The transmembrane (TM) segments are boxed and colored according to Figure 3. Outside the TM segments, sequence similarities are indicated by colored backgrounds (green background: hydrophobic residues; yellow: small or loop-forming residues; blue: basic; red: acidic; orange: aromatic). Within TM segments, only the non-hydrophobic residues, as well as proline and some conserved glycine residues, are shaded. Observed secondary structures (Sav1866) are indicated on top of the alignment. The TM and extracellular loop (ECL)/intracellular loop (ICL) numbering refers to the CFTR sequence. N-helix and C-helix indicate the N-terminal and C-terminal helices existing at the ends of the MSDs. The regions within ECLs, which could not be aligned, are displayed within gray boxes. Sav1866 (pdb 2HYD); MSBA (*E. coli* MsbA, Swiss-Prot P60752); CFTR (*H. sapiens* CFTR (ABCC7); Swiss-Prot P13569); MDR1 (*H. sapiens* MDR1 or P-glycoprotein 1 (ABCB1); Swiss-Prot P08183); SUR1 (*H. sapiens* SUR1 (ABCC8); Swiss-Prot Q09428); MRP1 (*H. sapiens* MRP1 (ABCC1); Swiss-Prot P33525); YOR1 (*S. cerevisiae* Yor1p; Swiss-Prot P53049).

large insertion (the regulatory insertion) was made in the CFTR sequence [5]. The resulting NBD1 model, constructed using as template the MJ0796 experimental structure [40], superimposed well with the experimental structure of mouse CFTR NBD1, which was published concomitantly [8]. This initial alignment was afterwards refined by taking into consideration an additional experimental structure (human TAP1, [41]) for modeling the ABC-specific α subdomain. This refinement led to a better fit with the experimental structure in the X-loop region preceding the ABC signature [6]. The X-loop region was defined after the experimental structure of Sav1866, in which it plays a key role in cross-linking the ICLs [21].

In the present work, the CFTR NBD1:NBD2 heterodimer model was constructed on the basis of its sequence alignment with the *S. aureus* Sav1866 sequence, which is characterized by a higher sequence identity level and tolerates less indels. The human CFTR NBD1 and NBD2 share, respectively, 25.6 % and 26.5 % sequence identity with the Sav1866 NBD. As previously reported, the CFTR NBD1 Walker A and Walker B motifs as well as the NBD2 signature sequence are highly modified relative to canonical ABC sequences [5, 6]. The CFTR NBD1/NBD2 heterodimer presents a head-to-tail orientation, with the two ATP-binding sites located at the interface between the two NBDs (Fig. 1A). The CFTR-specific large loop located between the strands β1 and β2 (regulatory insertion, in green in Fig. 1A) of NBD1 was modeled (with no indels), using as template the experimental 3-D structure of the isolated mouse CFTR NBD1 ([8], pdb 1r0z) for which only six amino acids in the middle of the loop are not seen in the crystal structure. This low number allows complete modeling of this long insertion {see Supplementary data 3 (http://www.impmc.jussieu.fr/~callebau/CFTR.html) for details of the loop building and for comparison with the regulatory insertion of the "hybrid" model of Serohijos et al. [39]}. In contrast, other NBD1 structures (*e.g.* 1r0w) are more limited and restricted to the N- and C-terminal parts of the loop, although they are completely coherent with the 1r0z structure. The structure of the NBD1:NBD2 heterodimer model was afterwards further energetically refined, in the context of the whole NBD:MSD assembly.

This Sav1866-based NBD heterodimer model shown in Figure 1A superimposes well with the Sav1866 experimental structure, as well as with our previous MJ0796/TAP1-based model of the NBD heterodimer [root mean square deviation (rmsd) 0.68 Å (450 superimposed Cα atoms) and 1.41 Å (397 superimposed Cα atoms), respectively]. The Sav1866-based model of human CFTR NBD1 also superimposes well with the crystal structure of the isolated human CFTR NBD1 [pdb 2bbo; 1.54 Å (276 superimposed Cα atoms)]. No fundamental differences were observed, although solubilizing mutations were introduced into NBD1 to allow the crystal structures to be obtained. These mutations are actually located outside the NBD1 structure core, in the regulatory insertion (F409L, F429S, F433L) and extension (R667H), or in the signature sequence region (G550E, R553Q, R555K), whose local conformations in the crystal structure and in our model are perfectly superimposable. Small local differences can, however, be observed in the solvent-accessible surface, in particular in regions participating in the NBD1:NBD2 and NBD1:MSDs interfaces, as well as in the relative orientation of the ABC-specific α−subdomain *versus* the α/β core (Supplementary data 1).

Membrane-spanning domains

The sequences of the human CFTR MSDs were aligned with those of several transporters of the ABCC (*e.g.*, MRP1 and SUR1) and ABCB (*e.g.*, MDR) families, as well as with those of Sav1866 and MsbA (Fig. 2). Most of the current modeling studies (*e.g.*, [26–30]) used TM segments and/or secondary structure predictions as main constraints for the alignments of these regions, which cannot be only based on sequence identity/similarity criteria. Here, in addition to these criteria, we used HCA [31–33], which allows the simultaneous consideration of primary and secondary structures. Although it is generally applied to globular domains, in which the secondary structures match well with the hydrophobic clusters delineated by the method, HCA has recently be proved to also be efficient for the alignment of TM segments of polytopic membrane proteins; in this case, typical large hydrophobic clusters contain small residues (alanine, glycine, threonine), playing an important role in the packing of the TM segments. This dichotomy and the associated topological features that can be deciphered on the 2-D HCA plot can be used to accurately align highly divergent sequences of TM segments (*e.g.* [34]; see the modeling of Rh proteins, based on the experimental structure of *E. coli* AmtB [35] and largely supported by the recent crystal structure of *Nitrosomonas europaea* Rh50 [36]).

In the case of the ABC transporters MSDs, anchor points for the alignment are furnished by the ICLs, as well as by the N-terminal and C-terminal helices, which are also on the cytoplasmic side of the membrane (Supplementary data 4; http://www.impmc.jussieu.fr/~callebau/CFTR.html). These regions possess hydrophobic clusters that are typical of globular domains and whose shapes are relatively

well conserved between the compared sequences [see the clusters (green) and the associated sequence identities in Supplementary data 4]. The TM segments form large hydrophobic clusters (boxed in Supplementary data 4), which can be aligned relative to the previously identified anchor points. This analysis led to the alignment presented in Figure 2, in which the TM segments are boxed. The human CFTR MSD1 and MSD2 sequences share 13.7% and 11.7% of sequence identity with the Sav1866 MSD, respectively. It can be noted that sequence identities are sometimes higher in the ICLs than in the TM segments [16.3% (ICL1), 16.9% (ICL2), 10.4% (ICL3) and 11.9% (ICL4)]. The resulting 3-D model is shown in Figures 1 and 3 (rmsd with Sav1866 0.67 Å – 632 superimposed Cα atoms). In Figure 3, the TM segments are colored according to Figure 2: the corresponding helices have the same color, but the MSD1 helices are dark-colored and the MSD2 helices light-colored. When compared to the model proposed by Serohijos et al. [39], our CFTR MSD model presents the following shifts in the TM helices : MSD1: TM1: shift of three CFTR amino acids towards the right (+3 aa); TM2: shift of two CFTR amino acids towards the left (–2 aa); TM3 : +1 aa; TM4: –1 aa; TM6 : –4 aa; MSD2: TM7: +3 aa; TM8: –8 aa; TM12: –6 aa. Only the alignments of TM5, TM9, TM10 and TM11 are identical between the two models. There are also significant differences in the alignments of the ICLs. In particular, the ICL1 coupling helix is shifted, as TM2, by two residues towards left (–2 aa) in our model relative to that of Serohijos et al., whereas the ascending helix towards TM3 is shifted of one residue towards right (+1 aa), as TM3. The descending helix from TM8 in ICL3 is also shifted of six residues towards left (–6 aa), TM8 being shifted of eight residues. In this helix, we propose a two-amino acid deletion at positions occupied in the multiple alignment by loop-forming residues, to satisfy the experimental constraint of an electrostatic interaction between R347 (TM6) and D924 (TM8) (see below). Finally, because of the shifts in the TM segments, discrepancies between the two models also exist in the extracellular loops (ECLs).

Our Sav1866-based model can be downloaded from http://www.impmc.jussieu.fr/~callebau/CFTR.html.

Results and discussion

General features of the MSD1:NBD1:MSD2:NBD2 assembly of human CFTR

According to our modeling strategy (see above), the MSDs of CFTR are expected to be arranged similarly to those of the Sav1866 homodimer (Fig. 1B). One of the most striking features of the Sav1866 MSD homodimer, in its outward-facing configuration, is the highly intricate association of the two half transporters, which involves the bundles of TM helices diverging into two wings, each containing the two first helices (TM1 and TM2) of one subunit and the four following ones (TM3 to TM6) of the other (a phenomenon termed swapping). It is, however, possible that the opening of this outward-facing configuration is more limited with CFTR than with Sav1866, because of the different nature of the substrates transported across the membrane. As discussed below, it may also be expected that the homologous helices of the two CFTR MSDs make rather asymmetric contributions to the pore, at least in the inward-facing conformation.

The helices of the MSD TM segments largely protrude into the cytoplasm to form ICLs, which possess at their most intracellular positions short helices (called "coupling helices") that run parallel to the plane of the membrane and physically interact with the NBDs (Fig. 1B). Of note, the above-discussed swapping of the TM helices leads to the interaction of the coupling helix of the second ICL (ICL2 in Sav1866, ICL2 and ICL4 in CFTR) with the NBD of the opposite subunit, while the coupling helix of the first ICL (ICL1 in Sav1866, ICL1 and ICL3 in CFTR) interacts with both NBD subunits (Fig. 1A). Finally, it is worth noting that the NBDs in the Sav1866 structure exhibit the conformation of the ATP-bound state, although ADP, rather than ATP, is bound [21].

Specific features of human CFTR MSD1:NBD1:MSD2:NBD2 assembly

Our previous work on the modeling of the CFTR NBD1:NBD2 heterodimer has demonstrated the amino acid residues that are essential for ATP binding and hydrolysis, and those involved in the heterodimer interface [5, 6]. Similarly, we first focus the present analysis on residues belonging to the TM segments within the MSDs, which may play a role in the functioning of the CFTR channel pore. Next, we focus on residues participating in the highly critical transmission interfaces between MSDs and NBDs; the role of NBD residues, for which new data have been obtained in the present modeling study, are therefore also discussed.

Membrane spanning domains

General features of the outward-facing conformation model. Previous CFTR mutagenesis studies performed to identify, within the TM helices, the residues lining the channel pore have revealed the important role of TM1, TM5, TM6 and TM12 ([42, 43] and

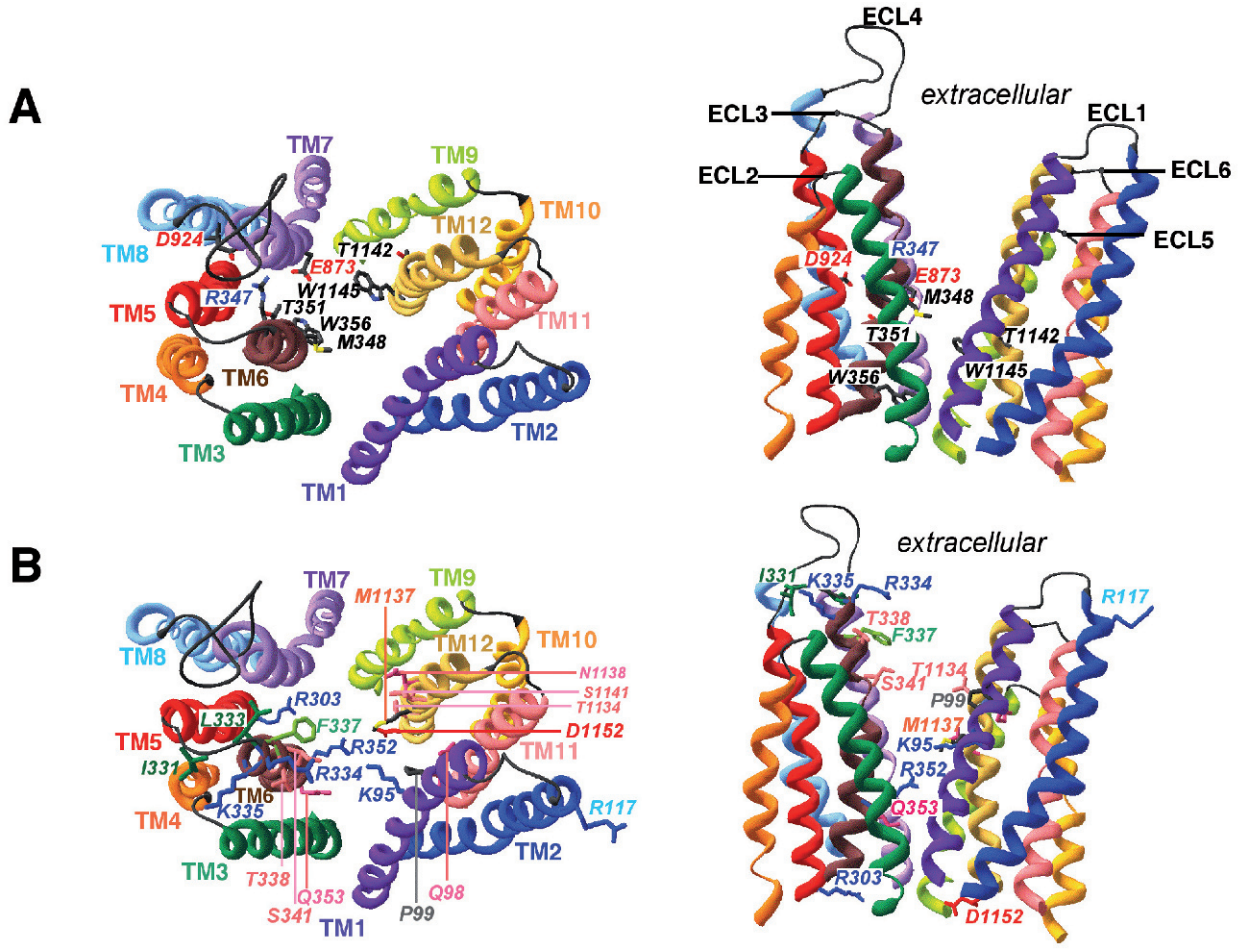

Figure 3. TM helices and ECLs viewed from the extracellular side (left) and from the membrane plane (right). (A) Residues highlighted by cysteine mutagenesis and disulfide cross-linking studies, as well as acidic and basic residues (labeled red and blue, respectively) that are likely to form electrostatic interactions. (B) Residues involved in channel structure and function. Residues are colored according to their physicochemical properties (blue = R, K; red = D, E; green = hydrophobic (I, L, F); pink = S, T, N, Q). Note the important length of ECL4, which contains N-glycosylation sites (Fig. 2).

references therein). As shown in Figure 3, these experimental data support a Sav1866-like overall organization of the CFTR membrane spanning segments, with a substrate translocation pathway lined at the outer leaflet of the membrane by TM1, TM3 and TM6 and their counterparts (TM7, TM9 and TM12) in MSD2.

It is worth noting here that, as already indicated above, the homologous helices of the MSDs may be expected to make rather asymmetric contributions to the channel. This hypothesis is based on the fact that (i) TM7 and TM11 seem to be less critical for the channel properties than TM1 and TM5 (references therein), and (ii) mutations in TM12 have fewer effects than those in TM6 [44]. Obviously, the CFTR model presented herein cannot account for such an asymmetry as it is based on the template of the Sav1866 symmetric transporter (Figs 1, 3). It should, however, be stressed that our model represents only one dynamic state of the transporter, its ATP-bound outward-facing configuration. This configuration likely maintains the overall symmetry observed in Sav1866, as the asymmetry in CFTR is supposed to be related to the lack of hydrolysis at one of the two ATP-binding sites (the NBD1 or non-canonical ATP-binding site). As a consequence, the presumed asymmetry of the CFTR MSDs might manifest itself during the conformational change following ATP hydrolysis at the canonical ATP binding site (NBD2 ATP-binding site), a change expected to lead to the return of the transporter to an inward-facing conformation [21]. This inward-facing conformation should thus lead to a greater participation of MSD1 than MSD2 helices in the channel functioning.

To further validate the accuracy of our model, we also analyzed the positions occupied by charged amino acid residues in the TM helices. It is noteworthy that, as expected for charged residues, the side chains of

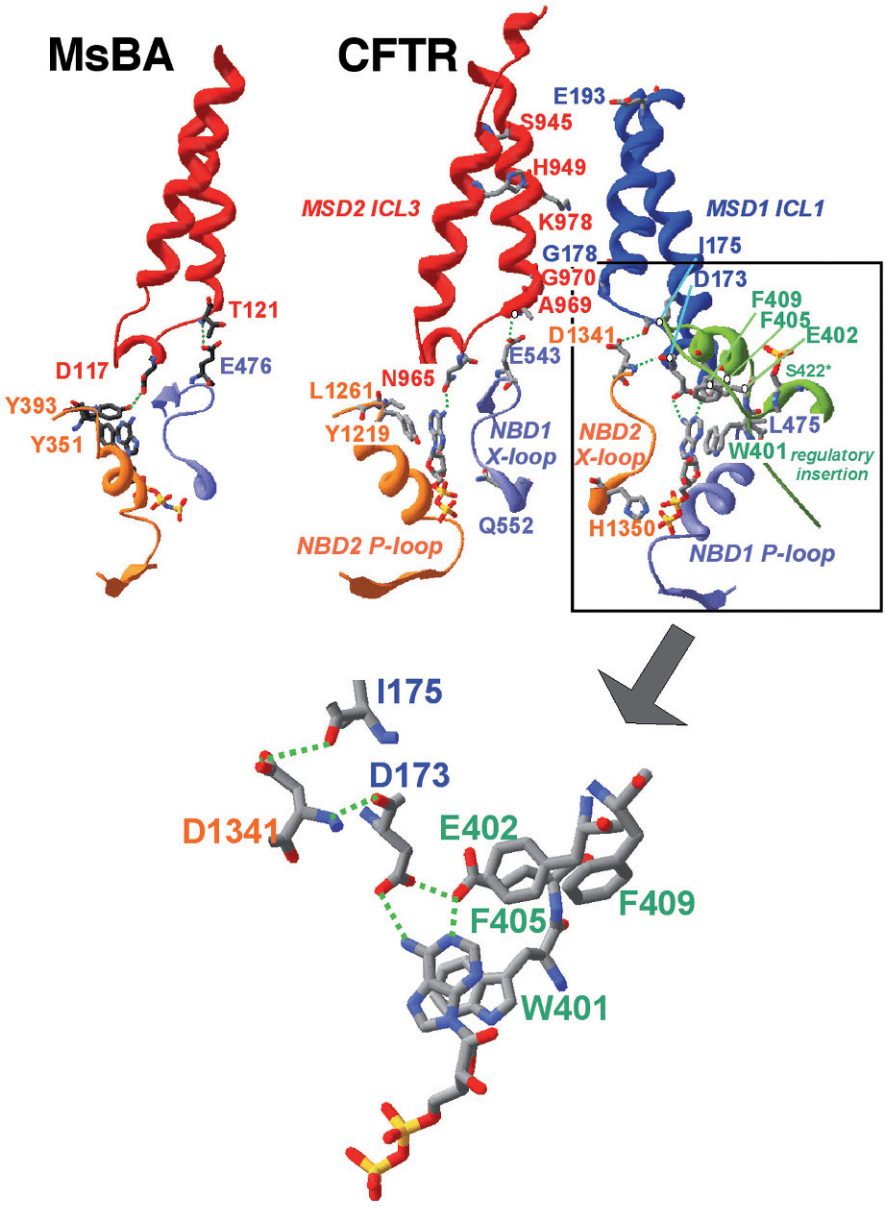

Figure 4. ICL1 and ICL3. View of the interface contacts between the NBD subunits and ICL1 (MSD1) or ICL3 (MSD2). MSD1 and NBD1 are colored dark and light blue, respectively, whereas MSD2 and NBD2 are colored red and orange, respectively. The NBD1 regulatory insertion is shown in green. The bound nucleotide is also indicated. S422* indicates the phosphorylated serine residue in the regulatory insertion. For comparison, one of the symmetrical ICL1/NBD contacts in *S. typhimurium* MsbA (pdb 3b60) is represented on the left.

most of them are indeed oriented towards the channel pore (E92 and K95 in TM1, R314 in TM2, R352 in TM6, E873 in TM7, D933 in TM9). Some residues are located at the inner border of the membrane, a position that allows them to expose their side chains on the cytoplasmic side of the bilayer (R242 at the end of TM4, R303 at the beginning of TM5, R933 at the end of TM8, R1097 at the beginning of TM11) (Fig. 3A). In addition, R347 in TM6 might form an electrostatic interaction with D924 in TM8, as well as with E873 in TM7 (see below). R1030 (TM10) may contact S1150 (end of TM12), whereas E1104 (TM11) might form a hydrogen bond (2.9 Å) with R134 (TM2).

Comparison with experimental data: disulfide cross-linking and channel function studies. The proximity of TM6 and TM12 was experimentally demonstrated by cysteine mutagenesis and disulfide cross-linking studies [10]. Interestingly, it appears that all the CFTR mutants for which disulfide cross-linking was detected (M348C in TM6 and T1142C in TM12; T351C in TM6 and T1142C in TM12; W356C in TM6 and W1145C in TM12) line the chloride channel pore and face each other (Fig. 3A). The conformational change leading to an inward-facing configuration might bring them sufficiently close to each other to allow a direct interaction. Although it has been reported that these constraints were also satisfied in the recent CFTR model proposed by Serohijos et al. (Fig. 6 in [39]), a

close comparison of the two models shows, for example, that the W356 side chain is well-oriented towards the channel pore in our model (Fig. 3A), while it is in a more buried position in the other model. Next, in light of our outward-facing, ATP-bound symmetrical model of CFTR, we examined the location of specific residues that have been shown to be involved in the functioning of the channel. We focused our analysis on residues from TM1, TM5, TM6 and TM12, which have been found to play a highly critical role. We therefore do not discuss mutagenesis experiments involving residues of other TMs (mainly TM3 residues [45]), although their results were generally also in good agreement with our model.

TM1 residues. In a study using a substituted cysteine accessibility method, residues G91, K95 and Q98 in TM1 were identified as lining the channel [46]. Moreover, mutation of K95 altered the permeability and/or conductance ratio for halides, suggesting that this residue is involved in the anion selectivity and permeation of the channel [1, 47]. A more recent study has confirmed and extended these results by indicating the role of K95 and Q98 in anion binding and that of K95, Q98 and P99 in unitary conductance and macroscopic current properties [43]. K95 has also been shown to attract permeant anions and open-channel blockers, such as glibenclamide [48]. In agreement with these observations, our model shows that the three aforementioned residues (G91, K95 and Q98) clearly line the channel, with the side chain of K95 protruding into the pore (Fig. 3B). Residue P99, which has been shown to contribute directly or indirectly to the channel function and also found mutated in CF [49], is also oriented in our model towards the pore, at the extremity of TM1 (Fig. 3B).

TM5 residues. Here, it was reported that mutations of G314 and V317 affect both anion permeation and channel gating [50, 51]. These residues are also orientated towards the pore, although the TM5 helix is rather distant from it (data not shown). Residue R303, whose side chain also protrudes into the channel pore (at its intracellular mouth as shown in Fig. 3B), has been reported to play an active role in the regulation of anion conduction *via* its positive charge [52] and to participate in a second open-channel blocker-binding site [53].

TM6 residues. Several mutagenesis studies have focused on the TM6 helix. Their results indicate that TM6 plays different key roles in the pore structure and function (unitary Cl^- channel conductance, anion selectivity, anion binding and channel gating; *e.g.*, [1, 44, 50, 54–64]). This helix contains several basic residues (R334, K335, R347 and R352), mutations of two of them (R334W and R347P) being associated with mild CF characterized by altered pore properties [63]. In our model, R334 and K335 are exposed in the outer vestibule, with the R334 side chain clearly protruding towards the mouth of the pore (Fig. 3B). R334 constitutes an important determinant of an anion-binding site in the extracellular mouth of the transporter [65]. The R352 side chain also projects well into the translocation pore (Fig. 3B). Only R347 appears to not directly participate in the pore, as it is oriented towards the MSD2 helices TM7 and TM8 (Fig. 3A). Accordingly, R347 mutations have been shown to destabilize the pore, but lead to a chloride flow similar to that of wild-type CFTR, suggesting that R347 does not interact directly with the permeating ions [66]. Subsequent mutagenesis work involving acidic residues located in different TM helices has shown that the D924R mutation could complement the R347D mutation, suggesting that these two residues may form a salt bridge. Our model satisfies this additional constraint and further indicates that R347 might also interact with the side chain of E873 in TM7 (Fig. 3A). Experimentally, R334 [63], K335 [64], R347 [63, 64] and R352 [52, 55] have been shown to be involved in Cl^- channel conductance, as well as F337 [55], T338 [59] and S341 [62]. It should be stressed here that the most dramatic effects were actually observed with these three last residues, which were thus believed to be located in a very narrow region of the pore. Here, Figure 3B shows that the side chains of F337, T338 and S341 are oriented towards the channel pore and might thus constitute a strangling in the channel, especially in its inward-facing configuration. In contrast to chloride channel conductance, which involves a whole series of amino acid residues, it was reported that anion selectivity (i) was mainly determined by two residues, F337 and T338, and (ii) could be modified by two other ones, R334 and S341 [57, 59, 67, 68]. Similarly to R334 [65], F337, T338 are also directly involved in the anion binding properties of CFTR [60]. Two mutations involving these residues (F337A and T338A) also significantly weakened the glibenclamide-mediated blocking of the channel [69], suggesting a direct interaction between the inhibitor and this region of the pore. Experimental work also showed that cysteine residues substituting for a series of TM6 residues (I331, L333, R334, K335, F337, S341, I344, R347, T351, R352, Q353) reacted with methanethiosulfonate (MTS) reagents, suggesting that these residues were water accessible [54, 70]. As regards the few residues that were not discussed above, it may be worth mentioning that Q353 appears well exposed within the pore (Fig. 3B). I331 and L333

are also found exposed, but rather lie within the extracellular loop 3 (ECL3).

TM12 residues. Investigating the functional importance of TM12, Gupta et al. [44] found that three mutations, affecting T1134, M1137 and S1141, significantly disrupted anion binding within the pore. These three residues project into the translocation pore of our CFTR model (Fig. 3B). There is a particularly good exposition of the M1137 side chain, which, on the contrary, is in a more buried configuration in the Serohijos model [39]. Mutations of T1134 and M1137 were found to also affect channel gating. However, in contrast to what was observed for TM6 residues, all the TM12 mutations studied had little effect on anion selectivity and unitary Cl^- conductance, suggesting asymmetric contributions of TM6 and TM12 to the pore functions [44]. Specific involvement of TM12 in CFTR gating suggests that this helix might be affected by a conformational change upon ATP-binding and hydrolysis at the canonical NBD2 site [44]. The fact that the CF-causing mutations M1137V, I1139V, D1152H and D1154G also interfere with the proper gating of the chloride channel [71] is in good agreement with such an hypothesis. In our model, the side chain of M1137 appears well exposed in the pore, as is also the case for D1152 (Fig. 3B), but this last residue belongs actually to the 'C-helix' helical extension (Fig. 2). Finally, two mutations of TM12 residues that also project towards the pore (N1138A and T1142A, Fig. 3B) were reported to significantly strengthen the glibenclamide block and to abolish its dependence on the extracellular Cl^- concentration [69], suggesting that these mutations may alter interactions between glibenclamide and Cl^- ions within the pore.

Residues within extracellular loops ECLs. The arginine R117 residue in ECL1 has been found to influence the channel properties and, accordingly, the well-known R117H mutation, which is generally associated with mild clinical disease, leads to reduced single-channel properties and open probability [63]. Interestingly, this residue lies exposed at the extracellular surface of the CFTR channel, but not at the entry of the pore (Fig. 3B). However, the rather long ECL1 is relatively close to ECL6 (~15 Å between R117 Cα and T1195 Cα), and it is thus possible that a direct interaction may occur between R117 and its neighboring ECL6, which, together with TM12, is probably the segment that moves the most during the conformational change leading to an inward conformation (J. P. Mornon et al., in preparation). Alternatively, R117 may be involved in critical relationships between CFTR and interacting proteins.

ICLs and MSDs:NBDs interfaces

ICL1:ICL3 and NBD ATP- binding sites / X-loops. According to our SAV1866-like architecture, the MSD1 ICL1 and MSD2 ICL3 interact with both NBDs (Fig. 1). First, an interaction can be observed between ICL1 or ICL3 and the P-loop region of the same NBD subunit (*i.e.*, NBD1 and NBD2, respectively), in a close proximity to the nucleotide ring. Our model suggests that the side chain of D173 in ICL1 may in fact directly interact with the N6 atom of the ATP adenine ring in the non-canonical NBD1 site (Fig. 4). A similar interaction can be observed between the corresponding N965 residue in ICL3 and the ATP adenine ring in the canonical NBD2 active site (Fig. 4). However, as regards the NBD1 ATP-binding site, it should be emphasized that an additional bond can be formed between the ATP N1 atom and the E402 glutamic acid, which is located in the beginning of the large regulatory insertion covering this non-canonical ATP-binding site and directly follows the tryptophan residue (W401) presumed to provide a stacking interaction with the ATP adenine ring (Fig. 4). Meanwhile, D173 and E402 may also directly interact with each other, as well as with S169 O (D173) and R170 O (E402). Such an interaction between ICL1 and the bound ATP molecule does not exist in Sav1866, as the amino acid corresponding to D173/N965 is an alanine (A113) (Fig. 2). An aspartic acid (D117) is also found in this position in *S. typhimurium* MsbA ICL1, but it is farther from the ATP ring and makes a hydrogen bond with the NBD Y393 of the same subunit (Fig. 4). Such an alternative bonding cannot exist in CFTR, as the CFTR residues equivalent to MsbA Y393 are leucines (L475 and L1261) (Fig. 4).

ICL1 and ICL3 also interact with the signature motif region of the opposite subunit, *i.e.*, NBD2 and NBD1, respectively (Fig. 1). Our model suggests that the main chain of ICL1 I175 and ICL3 A969 may indeed form a hydrogen bond with the lateral chain of an acidic residue located in the X-loop (located just before the signature sequence) of the opposite subunit, *i.e.*, D1341 in NBD2 and E543 in NBD1, respectively (Fig. 4). Note that an additional H bond can be formed between main chain atoms of D173 (O) and D1341 (N). A similar interaction with a conserved acidic residue of the X-loop is found in MsbA and Sav1866 (MsbA E476; Fig. 4) and has been proposed to allow transmission of the conformational changes occurring upon NBD ATP hydrolysis [21].

ICL2:NBD2 and ICL4:NBD1 interfaces. ICL2 and ICL4 make contacts with their opposite NBD subunits, the resulting ICL2:NBD2 and ICL4:NBD1

interfaces involving the NBD groove located between the α/β core and ABC-specific α sub-domain (Figs 1, 5). The main topology of these MSD:NBD interfaces appears actually to be conserved between Sav1866 and MsbA (Fig. 6), despite different atomic details. Key for these contacts are NBD1 F508, and its NBD2 counterpart, P1306 (Figs 5, 6).

As concerns the NBD1 F508 region, it is noteworthy that a very tight hydrogen bonding network may link the three side chain N atoms of ICL4 R1070 to (i) the oxygen atoms of the F508 and G509 main chain carbonyl groups, and (ii) the S511 side chain hydroxyl group (Fig. 5 and Supplementary data 5; http://www.impmc.jussieu.fr/~callebau/CFTR.html). The fact that a basic residue occupies this position in ICL4 is a specific feature of CFTR when compared to other transporters (see Fig. 2 where CFTR ICL4 R1070 is shown circled with a blue background), and it might thus represent a highly critical factor in the CFTR MSD:NBD interface. In addition, the aromatic side chains of other ICL4 residues (F1068, Y1073 and F1074) clearly also participate in this interface (Fig. 5). The ICL4 tryptophan W1063, which appears to be specific of CFTR (Fig. 2), may also participate in the ICL4/NBD1 interface (Fig. 5).

To gain some insights into how this ICL4/NBD1 interface may be modified upon F508 deletion, we superimposed the NBD1 structure of our Sav1866-based model with the experimental structure of ΔF508 NBD1 (pdb 1xmj; [9]) and locally substituted the C491-I521 segment. We then refined the entire model (Fig. 6). When F508 is deleted, most of the ICL4 R1070 hydrogen bonds with NBD1 disappear and only the I507 carbonyl group still favorably contacts the R1070 side chain NH_2 atom. In addition, the shortening of the polypeptidic chain also displaces V510 and S511 and, consequently, Y1073. Interestingly, it was very recently shown that the V510D mutation in the ΔF508 protein promotes its maturation [72]. This might be explained by the fact that the V510D mutation may restore the ICL4/NBD1 contacts missing in ΔF508. Indeed, as shown in Supplementary Data 6 (http://www.impmc.jussieu.fr/~callebau/CFTR.html), our refined model suggests that two novel, nearly symmetrical contacts [R1070 NH1 – D510 OD1 (3.0 Å); R1070 NH1 – D510 OD2 (3.3 Å)] may appear in V510D ΔF508. Along these lines, it is noteworthy that a folding defect similar to that of CFTR ΔF508 probably occurs in the case of the P-glycoprotein (P-gp or MDR1), where the ΔY490 deletion may also affect folding *via* a lack of ICL4/NBD1 contacts. However, the MDR1 position corresponding to CFTR R1070 is occupied by a glutamine residue (Q912, Fig. 2), which can make only one H bond with the F508 homolog in the NBD1 region [Y490 O (2.8 Å)], due to the chemical nature of its side chain (data not shown).

As regards the ICL2/NBD2 interface, it is worth noting that, similarly to the ICL4/NBD1 interface, the NBD2 residue (P1306) corresponding to F508 is in close proximity with the ICL2 W277 residue, which is the MSD1 counterpart of R1070 (data not shown). This ICL2/NBD2 interaction is reinforced by the contact between ICL2 Y275 and NBD2 Y1307.

Finally, it should be emphasized that Y1307, together with NBD2 aromatic residues (F1294 and F1296) and NBD1 aromatic residues (F508 and W496) constitute an aromatic groove at the surface of the NBD1/NBD2 heterodimer (Fig. 1A, right panel), as previously described in our NBD1/NBD2 model [6]. Thus, in light of the MSDs:NBDs model presented here, one may conclude that this aromatic groove, which also includes F490 and F494 (as highlighted in this study), defines the NBD binding sites of ICL2 and ICL4.

Naturally occurring mutations affecting ICL residues. The critical role of ICLs in the structure and function of CFTR is emphasized by the effects of naturally occurring mutations in these regions.

G178R (involving ICL1) and G970R (involving ICL3) are two CF-causing mutations. The G178R mutant exhibits impaired anion translocation capacity [73] and the G970R mutant is probably involved in obtaining or maintaining the open state of the transporter [74]. Interestingly, only glycine residues are found in the position occupied by these two equivalent residues in MSD1 and MSD2 (position highlighted with a black background in Fig. 2). This strictly conserved glycine residues appear to allow, because of their small size, a tight interaction of (i) ICL1 with ICL2 in the case of G178 and (ii) ICL3 with ICL4 in the case of G970 (Fig. 7). Indeed, in our CFTR model, substitution of G178 by any other residue results in a steric hindrance with the ICL2 main chain (3.5 Å between the Cα atoms of G178 and V260), while G970A is the only substitution that might be accommodated without steric incompatibility with ICL4 (4.7 Å between the Cα atoms of G970 and F1052) (Fig. 7).

Other CF-associated mutations of interest in ICL1 and ICL3 are (i) E193K, a mutation of an ICL1 residue that exhibits, similarly to G178R, impaired anion translocation capacity [73], and (ii) S945L, H949Y and G970R, which affect ICL3 residues and are probably involved (as G970R) in obtaining or maintaining the open state of the transporter [74]. These residues are located in the ascending helices leading to TM3 and TM9, respectively, and they are all oriented towards the translocation pore (Fig. 4). On the other hand, it is also interesting to note that K978 in ICL3, which is

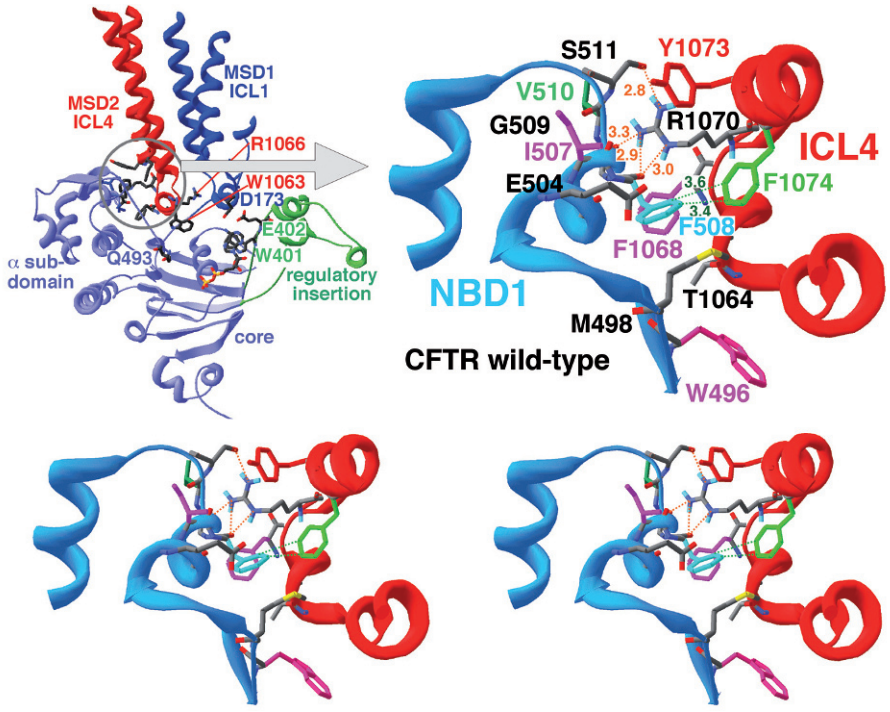

Figure 5. ICL2 and ICL4. Upper Left: View of the contacts established by the MSD2 ICL4 with NBD1 as well as with MSD1 ICL1 (viewed from the NBD heterodimer interface). Upper Right: Focus on the immediate neighborhood of F508. Bottom: the same view is displayed in a stereographical representation. Our model, built on the basis of the alignment shown in Figure 2 and in Supplementary data 1 (http://www.impmc.jussieu.fr/~callebau/CFTR.html), leads to a close contact between ICL4 and the NBD1 F508 region. F508 itself (side chain) is colored blue. One major feature of the NBD1:ICL4 interface is the presence of R1070, which is specific of CFTR (Fig. 2) and which is readily linked to the main chain CO carbonyl group of F508 *via* two symmetrically favorable H bonds (R1070 Nε to F508 O: 3.0 Å, Nε-H···O 144° – R1070 NH_2 to F508 O: 2.9 Å, NH_2-H···O 153°). Moreover, also nearly in the plane of the R1070, NH1 of the guanidinium group appears to establish a favorable H bond with the side chain of S511 (R1070 NH1 to S511 OG: 2.8 Å, NH1-H···O 139°) and NH2 a close contact with the G509 main chain carbonyl (R1070 NH2 to G509 O : 3.3 Å). Interestingly, the three C-O bonds (F508 C=O, G509 C=O and S511 C-OG) are nearly all parallel to each other and are distributed nearly perpendicularly to the R1070 guanidinium group, with their oxygens very close to its plane. Moreover, one can note that I507 C=O is also nearly bisector of the R1070 NH2-CZ-NH1 plane (O···NH2 3.3 Å, O···NH 3.9 Å) and that R1070 is maintained in this position by a close contact of NH1 and CD atoms with the Y1073 CB (3.7 Å and 4.0 Å, respectively; see Supplementary Data 4; http://www.impmc.jussieu.fr/~callebau/CFTR.html). In addition, the F508 side chain can establish favorable (~3.5 Å) Van der Waals contacts with F1074 (green dots) but remains, however, more distant from the other ICL4 neighbors (>4.9 Å for F1068, >6.0 Å for Y1073, >6.6 Å for T1064). Of note, F508 has also close contacts within NBD1 (~3.1 Å with the side chain of E504, ~3.3 Å with the side chain of M498).

also located in the ascending helix leading to TM9 and is oriented towards the translocation pore, was shown to be involved in CFTR inhibition by glibenclamide [75] (Fig. 4).

Naturally occurring mutations affecting ICL4 amino acids involved in contacts with the NBD1 F508 region have also been reported. Among these, several missense mutations have been observed for the critical R1070 residue (R1070W, R1070Q, R1070P; http://www.genet.sickkids.on.ca/cftr/), but no functional data are available for them. Functional information is only available for naturally occurring mutations of R1066, which generally disrupt either protein biosynthesis or channel gating [76, 77]. This basic amino acid residue R1066, which is highly conserved in the multiple alignments shown in Figure 2, interacts with the sequence linking MSD1 to NBD1 (data not shown).

In ICL2, the only missense mutation reported that was characterized at the functional level (R297Q) had little effect on the CFTR chloride channel activity [73]. Accordingly, the side chain of this amino acid does not participate in the channel and is exposed to the solvent at the cytoplasmic side of the membrane (data not shown).

General discussion and perspectives

The model of the MSD1:NDB1:MSD2:NBD2 assembly of human CFTR presented here is in good agreement with numerous experimental data available for this ABC transporter. This suggests that, in spite of intrinsic limitations due to the use of the Sav1866 structure as template (differences in substrates, in membrane environment, *etc.*), it may constitute a valuable basis for a better understanding of the molecular mechanisms associated with CFTR

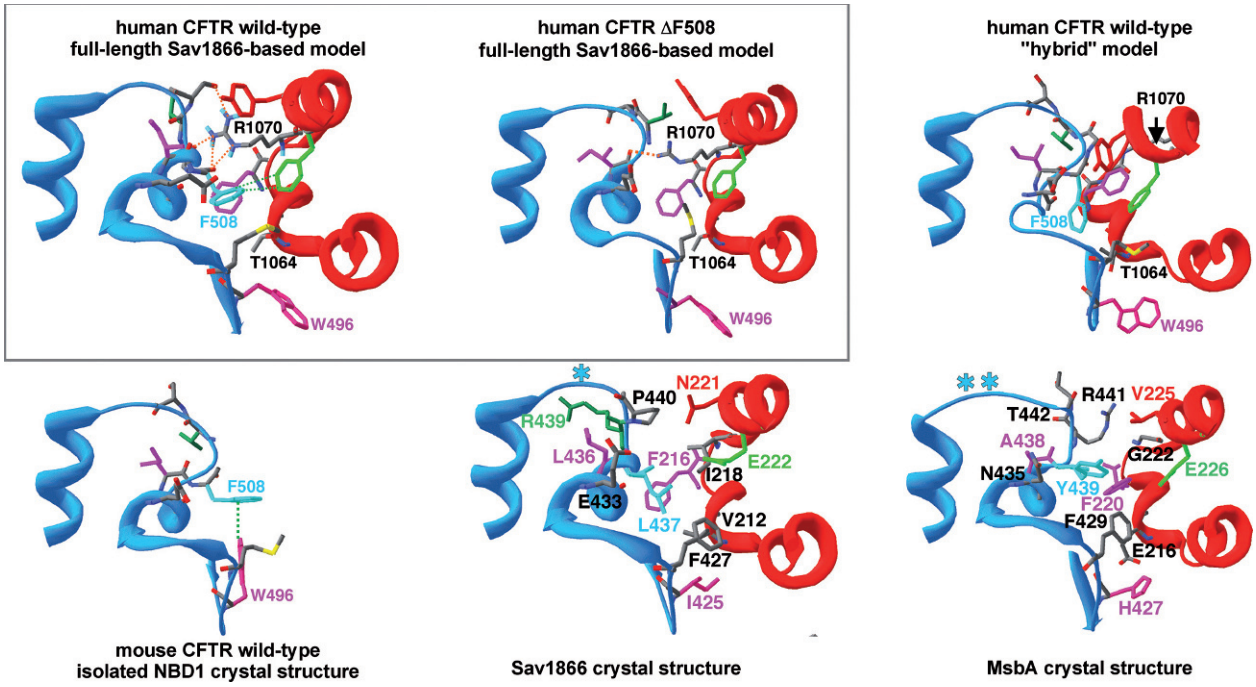

Figure 6. In the vicinity of F508. Comparison of our Sav1866-based CFTR model with: (i) our Sav1866-based ΔF508 model, (ii) the "hybrid" model of Serohijos et al. [39], (iii) a series of experimental structures (isolated mouse CFTR NBD1 [8], *S. aureus* Sav1866 [21] and *S. typhimurium* MsbA [25]). Top Left : Wild-type Sav1866-based CFTR model. The vicinity of F508 in our full-length Sav1866-based model of human CFTR is shown as in Figure 5. Top Middle: ΔF508. In order to unveil the structural modifications associated with F508 deletion, we superimposed the NDB1 structure of our Sav1866-based model with the experimental structure of ΔF508 NBD1 (pdb 1xmj; [9]) and locally substituted the C491–I521 segment of the wild-type model by that of the ΔF508 NBD1. We then refined the entire model. The resulting human CFTR ΔF508 model fits with the region shown here of the wild-type model (54 Cα positions) with a root mean square deviation (rmsd) of 1.53 Å. In the ΔF508 structure, most of the R1070 H bonds with NBD1 have disappeared; only the I507 carbonyl group still favorably contacts R1070 NH2 (3.1 Å, NH2-H···O 125°). In ΔF508, shortening of the peptide chain also displaces V510 and S511 and, consequently, Y1073. Top Right: "Hybrid" model [39]. The region of the polypeptidic chain shown here for this model fits our wild-type CFTR model with a rmsd of 2.34 Å (55 Cα positions). In this model, the main chains of NBD1 and ICL4 are clearly closer to each other and the R1070 residue is positioned at nearly 180° from its position in our model and is thus not in contact with NBD1. Also, some amino acids are close to the F508 side chain (*e.g.*, T1064 3.6 Å, F1068 2.9 Å, F1074 6.1 Å, Y1073 5.1 Å, M498 3.7 Å). Bottom. Experimental structures. (Left) Comparison of our Sav1866-based model with the experimental structure of an isolated NBD1 (mouse CFTR, [8]) shows major differences at the interface, obviously because of the lack of the interacting MSD partner. In particular, the important "face to edge" contact between W496 and F508 (~4.6 Å) totally disappears in the MSD:NBD assembly, as W496 adopts a new orientation (the former one being too close to T1064 (rmsd of 1.76 Å with our Sav1866-based model calculated for 51 Cα atoms)). (Middle and Right). 3-D crystal structures of the corresponding regions of *S. aureus* Sav1866, which has served as template for our modeling ([21]; pdb 2hyd; rmsd of 0.6 Å with our wild-type CFTR model – 55 Cα positions) and of *S. typhimurium* MsbA ([25]; pdb 3b60; rmsd of 1.51 Å with our wild-type CFTR model). In these crystal structures, there are one and two amino acids insertions, respectively, in the $\alpha_\alpha 1$- $\alpha_\alpha 2$ loop when compared to CFTR (blue stars; see also Supplementary data 1; http://www.impmc.jussieu.fr/~callebau/CFTR.html). This leads to a shorter loop in CFTR, allowing a positioning of the 507–509 main chain segment, which is adequate for interaction with R1070.

functions and also be used as a guide for further experimental characterization.

MSD:NBD interfaces

One of the fundamental differences between our modeling strategy and the recent work by Serohijos et al. [39], at least as regards the MSD:NBD interfaces, lies in the fact that we have solely used the entire Sav1866 structure [21] as template, whereas the Serohijos model was constructed on a 'hybrid' template, obtained by joining together the experimental structure of the Sav1866 MSDs [21], that of CFTR NBD1 [8] and our previously published model of CFTR NBD2 [5, 6]. It is indeed likely that the interactions existing at the MSD:NBD interfaces may be better estimated when one starts with an MSD:NBD assembly already fully characterized than with NBD1/NBD2 structures solved or predicted in absence of the MSDs (see Supplementary data 1 for a detailed comparison between the crystal structure of the isolated NBD1 structure and our Sav1866-based NBD1 model). Such a pure Sav1866-based modeling strategy allows the probable structural plasticity of the interface to be taken into account, while this is far more difficult when starting from isolated domain structures. It is thus not surprising that our model of the ICL2/ICL4:NBDs interfaces differs significantly from that of Serohijos et al., although the two

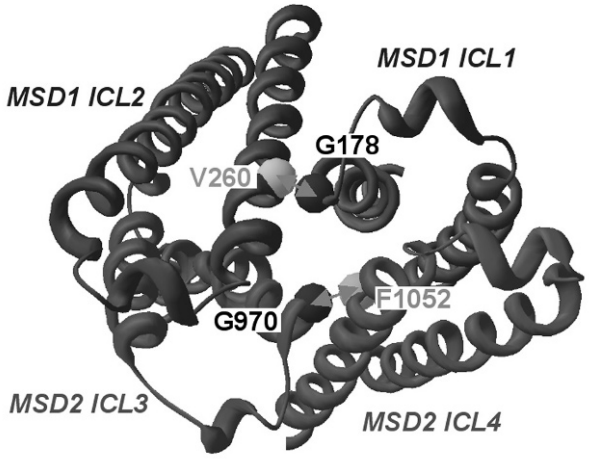

Figure 7. Contacts between ICLs. View of the closest contacts established by the MSD1 ICL1 with the MSD1 ICL2 (G178-V260) and by the MSD2 ICL3 with the MSD2 ICL4 (G970-F1052).

sequence alignments were identical in this region. In particular, the topological features of the ICL4 cluster of aromatic residues (F1068, Y1073 and F1074), which interact with the NBD1 F508 region are different between our model and that of Serohijos et al. [39] (Fig. 6). Our model also suggests that the interactions of ICL4 R1070 with main chain carbonyl groups of the NBD1 F508 region play a critical role in the ICL4/NBD1 interface; this also differs from the Serohijos model, in which the R1070 side chain was turned away from the interface (Fig. 6). Such a direct interaction between main chain atoms of the NBD1 F508 region and MSD2 R1070 may also help to explain why ΔF508 has a greater impact on the biosynthesis and function of CFTR than F508 missense mutations [78]. Thus, our model is in good agreement with the experimental work of Lewis et al. [9] showing that the deletion of F508 leads only to minimal changes of the NBD1 conformation and highlighting the role of the MSD/NBD interface in the folding deficiency of the ΔF508 protein. It is also worth noting here that the contacts between residues located on the NBD1 surface differ when NBD1 is analyzed as an isolated domain (wild type or ΔF508) from those encountered in the NBD:MSD complex (Fig. 6); this may explain the folding differences observed between the isolated domain and the whole complex [9, 78]. The tight binding of the F508 region with ICL4 may be of crucial importance during CFTR folding and its considerable weakening in the ΔF508 protein may thus constitute the mechanistic basis of the CFTR folding defect. This hypothesis is supported by the restoration of ΔF508 maturation by the V510D mutation [72]. Interestingly, a cavity can clearly be delineated at the NBD1:ICL4 interface of the ΔF508 protein, which is lined among others by ICL4 F1068 and NBD1 M498. Here, it is highly tempting to speculate that this cavity might be filled by a small aromatic molecule allowing the formation of novel hydrogen bonds between NBD1 and ICL4 (notably with R1070 NH2, T1064 OG1, N505 O and I506 O), and the subsequent correction of the CFTR folding defect.

The characteristics of the NBD interfaces with ICL1 and ICL3 also largely differ between our model and that of Serohijos et al. [39]. Here, the discrepancy probably originates from differences in the ICL1/ICL3 sequence alignments with the Sav1866 template. Interestingly, our alignment, which was refined using HCA (see Methods), led to highlight the potential role of an aspartic acid (D173) in ICL1 and of an asparagine (N965) in ICL3 for establishing H bonds with the ATP adenine rings (Fig. 4), as well as that of a strictly conserved glycine, G178 in ICL1 and G970 in ICL3, for forming tight contacts with ICL2 and ICL4, respectively (Fig. 7).

MSDs and channel pore

Several differences between our alignment and that of Serohijos et al. [39] are also observed in several TM helices of the MSDs. Although alignments may still be questionable in some regions, due to the very low levels of sequence identity, our model is largely supported by numerous experimental data available for critical MSD residues (see Results). Thus, our symmetric model of the outward-facing configuration of the CFTR channel most likely represents a realistic view of this state, as asymmetry is thought to be associated with the conformational changes leading to the inward-facing configuration. This outward-facing configuration clearly shows the importance of positively charged amino acid side chains in channel functioning. Accordingly, K95 in TM1 and R334 in TM6, which lie exposed at opposite ends of the TM segments (Fig. 3), probably play a critical role in attracting Cl^- into the channel pore [79]. As also suggested by our model, several ion-binding sites are present all along the pore (Fig. 3); this is in agreement with the hypothesis that the mechanism of chloride permeation may involve repulsive effects leading to high rates of Cl^- transport through the pore [79]. A region involving exposed TM6 residues (especially F337, T338, S341 [59, 67, 68]) was suggested to act as a selectivity filter and bind permeant ions [43, 56, 60]. This region might indeed form the narrowest part of the pore during the conformational change leading to an asymmetric inward-facing conformation of the MSDs. In addition, our study also permits to identify other potentially important residues, which might play a key role in CFTR channel functioning and have been identified as such in other ABC transporters. For

example, M348 in TM6, as well as W1145 in TM12 (the latter having been identified in cysteine mutagenesis and disulfide cross-linking studies [10]), appear well exposed in the pore and correspond to key residues of the MRP1 channel (F594 and W1246, respectively) [80, 81].

NBD ATP-binding sites

It should also be stressed that the model presented here does not only allow new insights into the probable architecture of the CFTR TM channel and the MSD:NBD interfaces, but also reciprocally permits further characterization of special features of the NBD ATP-binding sites. Our previous modeling study of the NBD1:NBD2 heterodimer has suggested that channel gating was mainly directed by ATP-binding and hydrolysis at the canonical NBD2 ATP-binding site, whereas ATP remains tightly bound, in a non-hydrolyzed form and for a long period, at the non-canonical NBD1 ATP-binding site [5]. This was consistent with different experimental studies performed on CFTR [82–84] and other asymmetric members of the ABC-C subfamily, such as MRP1 and SUR1 (reviewed in [5]).

Interestingly, the present model of the MSD1:NBD1:MSD2:NBD2 assembly clearly strengthens this asymmetrical behavior of the two ATP-binding sites, as it suggests that the non-conventional NBD1 ATP-binding site may actually be quite firmly locked, allowing a tight binding of ATP and preventing its release. This locking may indeed be ensured not only by the long regulatory insertion in the NBD1 ABC-specific β sub-domain, but also by several interactions with the ICLs (Figs 1, 4). First, as shown above, an acidic residue from ICL1 (D173) is likely to form a critical interaction with the ATP adenine ring, and possibly also with another acidic residue (E402) of the NBD1 regulatory insertion (Fig. 4). Main chain atoms of ICL1 residues, especially the carbonyl oxygen of the very same D173, are also likely to make hydrogen bonds with a conserved acidic residue (D1341) of the NBD2 X loop (Fig. 4). Most importantly, ICL1 also interacts with ICL4 and the side chain of ICL4 R1070 may form two hydrogen bonds with the carbonyl oxygen of NBD1 F508 (Fig. 5, upper left). Altogether, such an intricate network of interactions probably leads to a tight locking of the nucleotide at its non-conventional binding site. Moreover, it also suggests that F508, in addition to be a critical component of the NBD1:MSD2 interface, may play a role in the ATP stability within the non-conventional ATP-binding site.

Perspectives

The model described here should be of great help for conceiving experiments to gain a better understanding of the molecular basis of CF and for designing CFTR-specific drugs for its pharmacological treatment. Further advances that can yet be expected from theoretical studies may concern the modeling of the R domain, as well as that of the conformational changes leading to the inward-facing configuration of the transporter. In this last respect, the recent data on the revised structures of MsbA in a closed, inward-facing configuration [25] may help in gaining a better understanding of the mechanisms underlying this conformational change. It is likely that the asymmetry observed in the NBD heterodimer functioning may propagate towards the MSDs after ATP hydrolysis at the enzymatically-active NBD2 ATP-binding site. Thus, the conformational change leading to the inward-facing configuration of the transporter may involve a greater participation of MSD1 helices of the pore (especially TM1, TM3 and TM6) than of MSD2 helices (according to the mutagenesis data described above). On the other hand, the role of the R domain in the global architecture and function of CFTR remains to be further explored. Although the R domain is described as unrelated to any other protein and appears at first sight largely unstructured [85], our ongoing work suggests that, using sensitive methods of sequence analysis, it may be possible to find valuable templates on which the CFTR R domain can be modeled.

Acknowledgements. This work was supported by grants from the association "Vaincre La Mucoviscidose" (Paris, France).

1 Anderson, M. P., Gregory, R. J., Thompson, S., Souza, D. W., Paul, S., Mulligan, R. C., Smith, A. E. and Welsh, M. J. (1991) Demonstration that CFTR is a chloride channel by alteration of its anion selectivity. Science 253, 202–205.
2 Rowe, S. M., Miller, S. and Sorscher, E. J. (2005) Cystic fibrosis. N. Engl. J. Med. 352, 1992–2001.
3 Rowntree, R. K. and Harris, A. (2003) The phenotypic consequences of CFTR mutations. Ann. Hum. Genet. 67, 471–485.
4 Ostedgaard, L. S., Baldursson, O. and Welsh, M. J. (2001) Regulation of the cystic fibrosis transmembrane conductance regulator Cl^- channel by its R domain. J. Biol. Chem. 276, 7689–7692.
5 Callebaut, I., Eudes, R., Mornon, J. P. and Lehn, P. (2004) Nucleotide-binding domains of human cystic fibrosis transmembrane conductance regulator: Detailed sequence analysis and three-dimensional modeling of the heterodimer. Cell. Mol. Life Sci. 61, 230–242.
6 Eudes, R., Lehn, P., Férec, C., Mornon, J.-P. and Callebaut, I. (2005) Nucleotide binding domains of human CFTR: A structural classification of critical residues and disease-causing mutations. Cell. Mol. Life Sci. 62, 2112–2123.
7 Ambudkar, S. V., Kim, I. W., Xia, D. and Sauna, Z. E. (2006) The A-loop, a novel conserved aromatic acid subdomain upstream of the Walker A motif in ABC transporters, is critical for ATP binding. FEBS Lett. 580, 1049–1055.

8 Lewis, H. A., Buchanan, S. G., Burley, S. K., Conners, K., Dickey, M., Dorwart, M., Fowler, R., Gao, X., Guggino, W. B., Hendrickson, W. A., Hunt, J., Kearins, M. C., Lorimer, D., Maloney, P. C., Post, K. W., Rajashankar, K. R., Rutter, M. E., Sauder, J. M., Shriver, S., Thibodeau, P. H., Thomas, P. J., Zhang, M., Zhao, X. and Emtage, S. (2004) Structure of nucleotide-binding domain 1 of the cystic fibrosis transmembrane conductance regulator. EMBO J. 23 282–293.

9 Lewis, H. A., Zhao, X., Wang, C., Sauder, J. M., Rooney, I., Noland, B. W., Lorimer, D., Kearins, M. C., Conners, K., Condon, B., Maloney, P. C., Guggino, W. B., Hunt, J. F. and Emtage, S. (2005) Impact of the deltaF508 mutation in first nucleotide-binding domain of human cystic fibrosis transmembrane conductance regulator on domain folding and structure. J. Biol. Chem. 280, 1346–1353.

10 Chen, E. Y., Bartlett, M. C., Loo, T. W. and Clarke, D. M. (2004) The DeltaF508 mutation disrupts packing of the transmembrane segments of the cystic fibrosis transmembrane conductance regulator. J. Biol. Chem. 279, 39620–39627.

11 Cui, L., Aleksandrov, L., Chang, X. B., Hou, Y. X., He, L., Hegedus, T., Gentzsch, M., Aleksandrov, A., Balch, W. E. and Riordan, J. R. (2007) Domain interdependence in the biosynthetic assembly of CFTR. J. Mol. Biol. 365, 981–994.

12 Du, K., Sharma, M. and Lukacs, G. L. (2005) The DeltaF508 cystic fibrosis mutation impairs domain-domain interactions and arrests post-translational folding of CFTR. Nat. Struct. Mol. Biol. 12, 17–25.

13 Hollenstein, K., Dawson, J. P. and Locker, K. P. (2007) Structure and mechanism of ABC transporter proteins. Curr. Opin. Struct. Biol. 17, 412–418.

14 Locher, K. P., Lee, A. T. and Rees, D. C. (2002) The *E. coli* BtuCD structure: A framework for ABC transporter architecture and mechanism. Science 296, 1091–1098.

15 Chang, G. (2003) Structure of MsbA from *Vibrio cholera:* A multidrug resistance ABC transporter homolog in a closed conformation. J. Mol. Biol. 330, 419–430.

16 Chang, G. and Roth, C. B. (2001) Structure of MsbA from *E. coli:* A homolog of the multidrug resistance ATP binding cassette (ABC) transporters. Science 293, 1793–1800.

17 Reyes, C. L. and Chang, G. (2005) Structure of the ABC transporter MsbA in complex with ADP.vanadate and lipopolysaccharide. Science 308, 1028–1031.

18 Reyes, C. L., Ward, A., Yu, J. and Chang, G. (2006) The structures of MsbA: Insight into ABC transporter-mediated multidrug efflux. FEBS Lett. 580, 1042–1048.

19 Chang, G. (2007) Retraction of "Structure of MsbA from *Vibrio cholera:* A multidrug resistance ABC transporter homolog in a closed conformation" [J. Mol. Biol. (2003) 330, 419–430]. J. Mol. Biol. 369, 596.

20 Chang, G., Roth, C. B., Reyes, C. L., Pornillos, O., Chen, Y. J. and Chen, A. P. (2006) Retraction. Science 314, 1875.

21 Dawson, R. J. and Locher, K. P. (2006) Structure of a bacterial multidrug ABC transporter. Nature 443, 180–185.

22 Zolnerciks, J. K., Wooding, C. and Linton, K. J. (2007) Evidence for a Sav1866-like architecture for the human multidrug transporter P-glycoprotein. FASEB J. 21, 3937–3948.

23 Pinkett, H. W., Lee, A. T., Lum, P., Locher, K. P. and Rees, D. C. (2007) An inward-facing conformation of a putative metal-chelate-type ABC transporter. Science 315, 373–377.

24 Hollenstein, K., Frei, D. C. and Locher, K. P. (2007) Structure of an ABC transporter in complex with its binding protein. Nature 446, 213–216.

25 Ward, A., Reyes, C. L., Yu, J., Roth, C. B. and Chang, G. (2007) Flexibility in the ABC transporter MsbA: Alternating access with a twist. Proc. Natl. Acad. Sci. USA 104, 19005–19010.

26 DeGorter, M. K., Conseil, G., Deeley, R. G., Campbell, R. L. and Cole, S. P. (2008) Molecular modeling of the human multidrug resistance protein 1 (MRP1/ABCC1). Biochem. Biophys. Res. Commun. 365, 29–34.

27 Hazai, E. and Bikádi, Z. (2008) Homology modeling of breast cancer resistance protein (ABCG2). J. Struct. Biol. 162, 63–74.

28 Lawson, J., O'Mara, M. L. and Kerr, I. D. (2007) Structure-based interpretation of the mutagenesis database for the nucleotide binding domains of P-glycoprotein. Biochim. Biophys. Acta 1778, 376–391.

29 O'Mara, M. L. and Tieleman, D. P. (2007) P-glycoprotein models of the apo and ATP-bound states based on homology with Sav1866 and MalK. FEBS Lett. 581, 4217–4222.

30 Ravna, A. W., Sylte, I. and Sager, G. (2007) Molecular model of the outward facing state of the human P-glycoprotein (ABCB1), and comparison to a model of the human MRP5 (ABCC5). Theor. Biol. Med. Model 4, 33.

31 Callebaut, I., Labesse, G., Durand, P., Poupon, A., Canard, L., Chomilier, J., Henrissat, B. and Mornon, J. P. (1997) Deciphering protein sequence information through hydrophobic cluster analysis (HCA): Current status and perspectives. Cell. Mol. Life Sci. 53, 621–645.

32 Eudes, R., Le Tuan, K., Delettré, J., Mornon, J. P. and Callebaut, I. (2007) A generalized analysis of hydrophobic and loop clusters within globular protein sequences. BMC Struct. Biol. 7, 2.

33 Gaboriaud, C., Bissery, V., Benchetrit, T. and Mornon, J. P. (1987) Hydrophobic cluster analysis: An efficient new way to compare and analyse amino acid sequences. FEBS Lett. 224, 149–155.

34 Javadpour, M. M., Eilers, M., Groesbeek, M. and Smith, S. O. (1999) Helix packing in polytopic membrane proteins: Role of glycine in transmembrane helix association. Biophys. J. 77, 1609–1618.

35 Callebaut, I., Dulin, F., Bertrand, O., Ripoche, P., Mouro, I., Colin, Y., Mornon, J. P. and Cartron, J. P. (2006) Hydrophobic cluster analysis and modeling of the human Rh protein three-dimensional structures. Transfus. Clin. Biol. 13, 70–84.

36 Lupo, D., Li, X. D., Durand, A., Tomizaki, T., Cherif-Zahar, B., Matassi, G., Merrick, M. and Winkler, F. K. (2007) The 1.3-Å resolution structure of *Nitrosomonas europaea* Rh50 and mechanistic implications for NH3 transport by Rhesus family proteins. Proc. Natl. Acad. Sci. USA 104, 19303–19308.

37 Marti-Renom, M. A., Stuart, A., Fiser, A., Sánchez, R., Melo, F. and Sali, A. (2000) Comparative protein structure modeling of genes and genomes. Annu. Rev. Biophys. Biomol. Struct. 29, 291–325.

38 Guex, N. and Peitsch, M. C. (1997) SWISS-MODEL and the Swiss-PdbViewer: An environment for comparative protein modeling. Electrophoresis 18, 2714–2723.

39 Serohijos, A. W., Hegedus, T., Aleksandrov, A. A., He, L., Cui, L., Dokholyan, N. V. and Riordan, J. R. (2008) Phenylalanine-508 mediates a cytoplasmic-membrane domain contact in the CFTR 3D structure crucial to assembly and channel function. Proc. Natl. Acad. Sci. USA 105, 3256–3261.

40 Smith, P. C., Karpowich, N., Millen, L., Moody, J. E., Rosen, J., Thomas, P. J. and Hunt, J. F. (2002) ATP binding to the motor domain from an ABC transporter drives formation of a nucleotide sandwich dimer. Mol. Cell 10, 139–149.

41 Gaudet, R. and Wiley, D. C. (2001) Structure of the ABC ATPase domain of human TAP1, the transporter associated with antigen processing. EMBO J. 20, 4964–4972.

42 Frelet, A. and Klein, M. (2006) Insight in eukaryotic ABC transporter function by mutation analysis. FEBS Lett. 580, 1064–1084.

43 Ge, N., Muise, C. N., Gong, X. and Linsdell, P. (2004) Direct comparison of the functional roles played by different transmembrane regions in the cystic fibrosis transmembrane conductance regulator chloride channel pore. J. Biol. Chem. 279, 55283–55289.

44 Gupta, J., Evagelidis, A., Hanrahan, J. and Linsdell, P. (2001) Asymmetric structure of the cystic fibrosis transmembrane conductance regulator chloride channel pore suggested by mutagenesis of the twelfth transmembrane region. Biochemistry 40, 6620–6627.

45 Akabas, M. H. (1998) Channel-lining residues in the M3 membrane-spanning segment of the cystic fibrosis transmembrane conductance regulator. Biochemistry 37, 12233–12240.

46 Akabas, M. H., Kaufmann, C., Cook, T. A. and Archdeacon, P. (1994) Amino acid residues lining the chloride channel of the cystic fibrosis transmembrane conductance regulator. J. Biol. Chem. 269, 14865–14868.

47 Riordan, J. R., Rommens, J. M., Kerem, B., Alon, N., Rozmahel, R., Grzelczak, Z., Zielenski, J., Lok, S., Plavsic, N., Chou, J. L., Drumm, M. L., Iannuzzi, M. C., Collins, F. S. and Tsui, L. C. (1989) Identification of the cystic fibrosis gene: Cloning and characterization of complementary DNA. Science 245, 1066–1073.

48 Linsdell, P. (2005) Location of a common inhibitor binding site in the cytoplasmic vestibule of the cystic fibrosis transmembrane conductance regulator chloride channel pore. J. Biol. Chem. 280, 8945–8950.

49 Sheppard, D. N., Travis, S. M., Ishihara, H. and Welsh, M. J. (1996) Contribution of proline residues in the membrane-spanning domains of cystic fibrosis transmembrane conductance regulator to chloride channel function. J. Biol. Chem. 271, 14995–15001.

50 Mansoura, M. K., Smith, S. S., Choi, A. D., Richards, N. W., Strong, T. V., Drumm, M. L., Collins, F. S. and Dawson, D. C. (1998) Cystic fibrosis transmembrane conductance regulator (CFTR) anion binding as a probe of the pore. Biophys. J. 74, 1320–1332.

51 Zhang, Z. R., Zeltwanger, S., Smith, S. S., Dawson, D. C. and McCarty, N. A. (2002) Voltage-sensitive gating induced by a mutation in the fifth transmembrane domain of CFTR. Am. J. Physiol. Lung Cell. Mol. Physiol. 282, L135-L145.

52 St Aubin, C. N. and Linsdell, P. (2006) Positive charges at the intracellular mouth of the pore regulate anion conduction in the CFTR chloride channel. J. Gen. Physiol. 128, 535–545.

53 St Aubin, C. N., Zhou, J. J. and Linsdell, P. (2007) Identification of a second blocker binding site at the cytoplasmic mouth of the cystic fibrosis transmembrane conductance regulator chloride channel pore. Mol. Pharmacol. 71, 1360–1368.

54 Cheung, M. and Akabas, M. H. (1996) Identification of cystic fibrosis transmembrane conductance regulator channel-lining residues in and flanking the M6 membrane-spanning segment. Biophys. J. 70, 2688–2699.

55 Guinamard, R. and Akabas, M. H. (1999) Arg352 is a major determinant of charge selectivity in the cystic fibrosis transmembrane conductance regulator chloride channel. Biochemistry 38, 5528–5537.

56 Linsdell, P. (2001) Relationship between anion binding and anion permeability revealed by mutagenesis within the cystic fibrosis transmembrane conductance regulator chloride channel pore. J. Physiol. 531, 51–66.

57 Linsdell, P., Evagelidis, A. and Hanrahan, J. W. (2000) Molecular determinants of anion selectivity in the cystic fibrosis transmembrane conductance regulator chloride channel pore. Biophys. J. 78, 2973–2982.

58 Linsdell, P., Tabcharani, J. A., Rommens, J. M., Hou, Y. X., Chang, X. B., Tsui, L. C., Riordan, J. R. and Hanrahan, J. W. (1997) Permeability of wild-type and mutant cystic fibrosis transmembrane conductance regulator chloride channels to polyatomic anions. J. Gen. Physiol. 110, 355–364.

59 Linsdell, P., Zheng, S. X. and Hanrahan, J. W. (1998) Non-pore lining amino acid side chains influence anion selectivity of the human CFTR Cl- channel expressed in mammalian cell lines. J. Physiol. 512, 1–16.

60 Gong, X., Burbridge, S. M., Cowley, E. A. and Linsdell, P. (2002) Molecular determinants of Au(CN)(2)(-) binding and permeability within the cystic fibrosis transmembrane conductance regulator Cl(-) channel pore. J. Physiol. 540, 39–47.

61 McCarty, N. A. (2000) Permeation through the CFTR chloride channel. J. Exp. Biol. 203, 1947–1962.

62 McDonough, S., Davidson, N., Lester, H. A. and McCarty, N. A. (1994) Novel pore-lining residues in CFTR that govern permeation and open-channel block. Neuron 13, 623–634.

63 Sheppard, D. N., Rich, D. P., Ostedgaard, L. S., Gregory, R. J., Smith, A. E. and Welsh, M. J. (1993) Mutations in CFTR associated with mild-disease-form Cl- channels with altered pore properties. Nature 362, 160–164.

64 Tabcharani, J. A., Rommens, J. M., Hou, Y. X., Chang, X. B., Tsui, L. C., Riordan, J. R. and Hanrahan, J. W. (1993) Multi-ion pore behaviour in the CFTR chloride channel. Nature 366, 79–82.

65 Gong, X. and Linsdell, P. (2003) Molecular determinants and role of an anion binding site in the external mouth of the CFTR chloride channel pore. J. Physiol. 549, 387–397.

66 Cotten, J. F. and Welsh, M. J. (1999) Cystic fibrosis-associated mutations at arginine 347 alter the pore architecture of CFTR. Evidence for disruption of a salt bridge. J. Biol. Chem. 274, 5429–5435.

67 McCarty, N. A. and Zhang, Z. R. (2001) Identification of a region of strong discrimination in the pore of CFTR. Am. J. Physiol. Lung Cell. Mol. Physiol. 281, L852-L867.

68 Gupta, J. and Lindsell, P. (2003) Extent of the selectivity filter conferred by the sixth transmembrane region in the CFTR chloride channel pore. Mol. Membr. Biol. 20, 45–52.

69 Gupta, J. and Linsdell, P. (2002) Point mutations in the pore region directly or indirectly affect glibenclamide block of the CFTR chloride channel. Pflugers Arch. 443, 739–747.

70 Cheung, M. and Akabas, M. H. (1997) Locating the anion-selectivity filter of the cystic fibrosis transmembrane conductance regulator (CFTR) chloride channel. J. Gen. Physiol. 109, 289–299.

71 Vankeerberghen, A., Wei, L., Teng, H., Jaspers, M., Cassiman, J. J., Nilius, B. and Cuppens, H. (1998) Characterization of mutations located in exon 18 of the CFTR gene. FEBS Lett. 437, 1–4.

72 Wang, Y., Loo, T. W., Bartlett, M. C. and Clarke, D. M. (2007) Correctors promote maturation of cystic fibrosis transmembrane conductance regulator (CFTR)-processing mutants by binding to the protein. J. Biol. Chem. 282, 33247–33251.

73 Seibert, F. S., Jia, Y., Mathews, C. J., Hanrahan, J. W., Riordan, J. R., Loo, T. W. and Clarke, D. M. (1997) Disease-associated mutations in cytoplasmic loops 1 and 2 of cystic fibrosis transmembrane conductance regulator impede processing or opening of the channel. Biochemistry 36, 11966–11974.

74 Seibert, F. S., Linsdell, P., Loo, T. W., Hanrahan, J. W., Riordan, J. R. and Clarke, D. M. (1996) Cytoplasmic loop three of cystic fibrosis transmembrane conductance regulator contributes to regulation of chloride channel activity. J. Biol. Chem. 271, 27493–27499.

75 Melin, P., Hosy, E., Vivaudou, M. and Becq, F. (2007) CFTR inhibition by glibenclamide requires a positive charge in cytoplasmic loop three. Biochim. Biophys. Acta 1768, 2438–2446.

76 Cotten, J. F., Ostedgaard, L. S., Carson, M. R. and Welsh, M. J. (1996) Effect of cystic fibrosis-associated mutations in the fourth intracellular loop of cystic fibrosis transmembrane conductance regulator. J. Biol. Chem. 271, 21279–21284.

77 Seibert, F. S., Linsdell, P., Loo, T. W., Hanrahan, J. W., Clarke, D. M. and Riordan, J. R. (1996) Disease-associated mutations in the fourth cytoplasmic loop of cystic fibrosis transmembrane conductance regulator compromise biosynthetic processing and chloride channel activity. J. Biol. Chem. 271, 15139–15145.

78 Thibodeau, P. H., Brautigam, C. A., Machius, M. and Thomas, P. J. (2005) Side chain and backbone contributions of Phe508 to CFTR folding. Nat. Struct. Mol. Biol. 12, 10–16.

79 Linsdell, P. (2006) Mechanism of chloride permeation in the cystic fibrosis transmembrane conductance regulator chloride channel. Exp. Physiol. 91, 123–129.

80 Campbell, J. D., Koike, K., Moreau, C., Sansom, M. S., Deeley, R. G. and Cole, S. P. (2004) Molecular modeling correctly predicts the functional importance of Phe594 in transmembrane helix 11 of the multidrug resistance protein, MRP1 (ABCC1). J. Biol. Chem. 279, 463–468.

81 Ito, K., Olsen, S. L., Qiu, W., Deeley, R. G. and Cole, S. P. (2001) Mutation of a single conserved tryptophan in multidrug resistance protein 1 (MRP1/ABCC1) results in loss of drug

resistance and selective loss of organic anion transport. J. Biol. Chem. 276, 15616–15624.
82 Aleksandrov, L., Aleksandrov, A. A., Chang, X. B. and Riordan, J. R. (2002) The first nucleotide binding domain of cystic fibrosis transmembrane conductance regulator is a site of stable nucleotide interaction, whereas the second is a site of rapid turnover. J. Biol. Chem. 277, 15419–15425.
83 Basso, C., Vergani, P., Nairn, A. C. and Gadsby, D. C. (2003) Prolonged nonhydrolytic interaction of nucleotide with CFTR's NH_2-terminal nucleotide binding domain and its role in channel gating. J. Gen. Physiol. 122, 333–348.
84 Gunderson, K. L. and Kopito, R. R. (1995) Conformational states of CFTR associated with channel gating: The role ATP binding and hydrolysis. Cell 82, 231–239.
85 Baker, J. M., Hudson, R. P., Kanelis, V., Choy, W. Y., Thibodeau, P. H., Thomas, P. J. and Forman-Kay, J. D. (2007) CFTR regulatory region interacts with NBD1 predominantly *via* multiple transient helices. Nat. Struct. Mol. Biol. 14, 738–745.